Two-dimensional modeling of high-velocity impingement of polymethylmethacrylate plates

T V Popova[1], A E Mayer[1] and K V Khishchenko[2]

[1] Chelyabinsk State University, Bratiev Kashirinykh Street 129, Chelyabinsk 454001, Russia
[2] Joint Institute for High Temperatures of the Russian Academy of Sciences, Izhorskaya 13 Bldg 2, Moscow 125412, Russia

E-mail: tatyana_maskaeva@mail.ru

Abstract. Using modification of Maxwell model of viscoelastic medium, we have performed 2D simulations of the polymethylmethacrylate (PMMA) plates impingement at high velocities. Previously, we had investigated numerically the influence of the viscoelastic properties upon the dynamics of 1D shock-wave flows in PMMA. It was shown that, in a limit of weak shock waves, the accounting of the viscoelastic properties allows one to achieve a better agreement of calculated results and experimental data on the shock wave velocity magnitude than in the case of hydrodynamic calculations. In the present work, we make a generalization of the polymer material deformation model to the case of 2D stress state. The equation is written for the plastic deformation tensor, which describes the relaxation of the maximal shear stress.

1. Introduction

High-molecular compounds (polymers) represent a valuable class of materials. The interest in studying of the process of dynamic behavior of polymers, in particular polymethylmethacrylate (PMMA), is due to the fact that these materials have unique combination of properties and are widely used in various fields of science and technology. Many physical phenomena associated with the dynamic deformation of polymeric materials are accompanied by the formation and interaction of shock waves [1]. The impact of plates with known velocities creates well controlled conditions of loading. A number of experimental works is devoted to study of deformation and destruction of PMMA at quasi-static and dynamic loading [2–7]. An important phenomenon of the shock-wave dynamics in the loaded material is the effect of spallation [8]. To determine the spall strength of the material, some authors [5–7] use the approach based on the measuring the depth of the resulting cave, left by the spalled piece after the intensive pulsed laser action on the target, and the velocity of the spalled layer with the subsequent mathematical modeling of the shock-wave process within the studied target [9]. This approach is sensitive to that how correctly the dynamics of the shock wave is calculated. The Mises condition and Maxwell model was combined in the work [10] for a polymer. In the present work, we use the Coulomb–Tresca approach, where the plastic deformation is caused by the relaxation of the maximum shear stress.

We had already investigated numerically the influence of the viscoelastic properties on the shock wave dynamics in PMMA in 1D simulations previously [11]. It was shown that, in a limit of weak shock waves, the accounting of the viscoelastic properties allows one to achieve a better agreement of calculated results and experimental data on the magnitude of the shock wave

velocity than in the case of hydrodynamic simulations. The results showed that the changes of the shock wave amplitude with the depth are approximately identical in the hydrodynamic and viscoelastic cases. In this work, we present a generalization of the polymer material deformation model.

2. Mathematical model

The basic system of equations of continuum mechanics [12] in 2D is as follows:

$$\frac{\mathrm{d}\rho}{\mathrm{d}t} = -\rho\frac{\partial \upsilon_k}{\partial x_k}, \tag{1}$$

$$\rho\frac{\mathrm{d}\upsilon_i}{\mathrm{d}t} = \frac{\partial \sigma_{ik}}{\partial x_k} + \eta_1 \Delta \upsilon_i, \tag{2}$$

$$\rho\frac{\mathrm{d}E}{\mathrm{d}t} = \sigma_{ik}\upsilon_{ik}, \tag{3}$$

where υ_i is the substance velocity; ρ is the density; $\sigma_{ik} = -P\delta_{ik} + S_{ik}$ is the combined stress; P is the pressure; S_{ik} is the stress deviator; η_1 is the coefficient of viscosity, E is the internal energy. The system consists of equation of continuity (1), equation of motion (2) and equation for the internal energy (3). Caloric equation of state [13, 14] is used to calculate the dependence of pressure upon the specific volume $V = 1/\rho$ and the specific internal energy E. The system should be added with an equation for the stress deviator (Hooke's law) [15]:

$$S_{ik} = 2G\left[u_{ik} - \frac{1}{3}\delta_{ik}u_{ll} - W_{ik}\right], \tag{4}$$

where $u_{ll} = u_{xx} + u_{yy}$; W_{ik} is the component of the plastic strain tensor; G is the shear modulus; u_{ik} is the component of the macroscopic strain tensor, which is defined by the macroscopic motion of matter:

$$\frac{\mathrm{d}u_{ik}}{\mathrm{d}t} = \frac{1}{2}\left(\upsilon_{ik} + \upsilon_{ki}\right) + o_{ik}, \quad \upsilon_{ik} = \frac{\partial \upsilon_i}{\partial x_k}. \tag{5}$$

The term o_{ik} takes into account the volume element rotation relative to the coordinate system. We refer the velocity, pressure and density to the certain particles of the continuous medium moving in space in the course of time.

3. Model of viscoelasticity

3.1. 1D model

Using the Maxwell model of viscoelastic medium, we consider the uniaxial deformation of the material. At the series connection, tension in each element is the same, while the general deformation consists of deformation of the elastic element and deformation of the viscous one. In this case, we can write [15]

$$\frac{\mathrm{d}S_{xx}}{\mathrm{d}t} = G\left(\frac{4}{3}\frac{\mathrm{d}u_{xx}}{\mathrm{d}t} - \frac{S_{xx}}{\eta}\right), \tag{6}$$

where η is the coefficient of viscosity. Substituting the stress deviator in equation (6) we can find an equation for the plastic deformation

$$\frac{\mathrm{d}W_{xx}}{\mathrm{d}t} = \left(\frac{2}{3}u_{xx} - W_{xx}\right)\tau^{-1}, \tag{7}$$

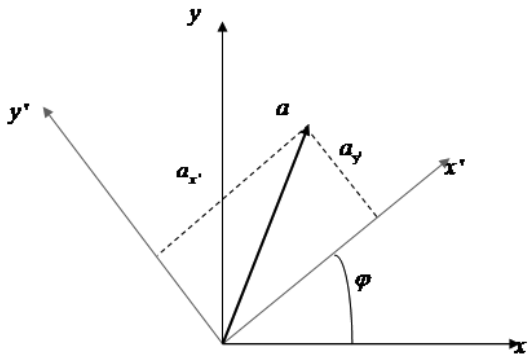

Figure 1. Laboratory and auxiliary coordinate systems.

where $\tau = \eta/G$ is the relaxation time. The plastic flow in polymers starts at the value of the stress deviator S_{xx} larger than the threshold y_b characterizing the static yield stress; generalization of equation (7) is as follows [11]:

$$\frac{\mathrm{d}W_{xx}}{\mathrm{d}t} = \left(\frac{2}{3}u_{xx} - W_{xx} - \frac{y_b}{2G}\right)\tau^{-1} \times \theta\left(|S_{xx}| - y_\mathrm{b}\right), \tag{8}$$

where θ is the Heaviside function. The main stress axes coincide with the x, y, z axes.

3.2. 2D model

The purpose of this section is to determine the component of the plastic strain tensor using a model of viscoelasticity. We generalize the equation (8), written in the main axes in the two-dimensional case. Rotation is necessary to go to the main axes.

Let us consider the auxiliary coordinate system (primed) rotated relative to the laboratory coordinate system by the angle φ (figure 1). Expressing the new coordinates through old one, we find the relationship between the coordinates of the same point in different coordinate systems on a plane:

$$\begin{pmatrix} a_{x'} \\ a_{y'} \end{pmatrix} = \begin{pmatrix} \cos\varphi & \sin\varphi \\ -\sin\varphi & \cos\varphi \end{pmatrix} \begin{pmatrix} a_x \\ a_y \end{pmatrix}. \tag{9}$$

Similarly, we can write for the stress deviator:

$$\begin{pmatrix} S_{x'x'} & S_{x'y'} \\ S_{x'y'} & S_{y'y'} \end{pmatrix} = \begin{pmatrix} \cos\varphi & -\sin\varphi \\ \sin\varphi & \cos\varphi \end{pmatrix} \begin{pmatrix} S_{xx} & S_{xy} \\ S_{xy} & S_{yy} \end{pmatrix} \begin{pmatrix} \cos\varphi & \sin\varphi \\ -\sin\varphi & \cos\varphi \end{pmatrix}. \tag{10}$$

After multiplication, we obtain the following expression for the component $x'y'$:

$$S_{x'y'} = S_{xx}\sin\varphi\cos\varphi + S_{xy}\cos^2\varphi - S_{xy}\sin^2\varphi - S_{yy}\sin\varphi\cos\varphi. \tag{11}$$

Go to the system of the main axes, where the nondiagonal components must be equal to zero:

$$S_{x'y'} = \frac{1}{2}\sin(2\varphi)(S_{xx} - S_{yy}) + S_{xy}\cos(2\varphi) = 0. \tag{12}$$

In this way, we find an expression for the angle:

$$\tan(2\varphi) = \frac{2S_{xy}}{S_{yy} - S_{xx}}, \tag{13}$$

$$\varphi = \frac{1}{2}\arctan\left(\frac{2S_{xy}}{S_{yy}-S_{xx}}\right). \tag{14}$$

From (10), after multiplication, we obtain the following expression for the component $S_{x'x'}$:

$$\begin{aligned} S_{x'x'} &= S_{xx}\cos^2\varphi - 2S_{xy}\sin\varphi\cos\varphi + S_{yy}\sin^2\varphi, \\ S_{x'x'} &= \frac{1}{2}(S_{yy}+S_{xx}) + \frac{1}{2}(S_{xx}-S_{yy})\cos(2\varphi) - S_{xy}\sin(2\varphi). \end{aligned} \tag{15}$$

Taking into account equality

$$\cos(2\varphi) = \pm\frac{1}{\sqrt{1+\tan^2(2\varphi)}}, \quad \sin(2\varphi) = \pm\frac{\tan(2\varphi)}{\sqrt{1+\tan^2(2\varphi)}}, \tag{16}$$

and relation (13), we obtain after several transformations the following expression:

$$S_{x'x'} = \frac{1}{2}(S_{yy}+S_{xx}) + \frac{1}{2}\sqrt{(S_{yy}-S_{xx})^2 + 4S_{xy}^2}. \tag{17}$$

Similarly, for the component $S_{y'y'}$:

$$S_{y'y'} = \frac{1}{2}(S_{yy}+S_{xx}) - \frac{1}{2}\sqrt{(S_{yy}-S_{xx})^2 + 4S_{xy}^2}. \tag{18}$$

Using formulas (17) and (18), we find the maximum tangential stress, which is equal to half of the absolute value of the main stresses:

$$\sigma_\tau = \frac{S_{x'x'} - S_{y'y'}}{2}. \tag{19}$$

Differential formulation of plastic strain tensor that determines the shear stress via Hooke's law (4) takes the following form:

$$\frac{\mathrm{d}W_{x'x'}}{\mathrm{d}t} = \frac{1}{2G\tau}\left(\frac{4}{3}\sigma_\tau - y_b\right) \times \theta\left(\frac{4}{3}|\sigma_\tau| - y_b\right). \tag{20}$$

Plastic deformation preserves the volume, therefore assuming $W_{z'z'} = 0$, we will have

$$\frac{\mathrm{d}W_{x'x'}}{\mathrm{d}t} = -\frac{\mathrm{d}W_{y'y'}}{\mathrm{d}t}.$$

Expressing the new value through old one, we find the relationship between the values in the same point in different coordinate systems on the plane:

$$\begin{pmatrix} \mathrm{d}W_{xx}/\mathrm{d}t & \mathrm{d}W_{xy}/\mathrm{d}t \\ \mathrm{d}W_{xy}/\mathrm{d}t & \mathrm{d}W_{yy}/\mathrm{d}t \end{pmatrix} = \begin{pmatrix} \cos\varphi & -\sin\varphi \\ \sin\varphi & \cos\varphi \end{pmatrix} \begin{pmatrix} \mathrm{d}W_{x'x'}/\mathrm{d}t & 0 \\ 0 & -\mathrm{d}W_{x'x'}/\mathrm{d}t \end{pmatrix} \begin{pmatrix} \cos\varphi & \sin\varphi \\ -\sin\varphi & \cos\varphi \end{pmatrix}. \tag{21}$$

After multiplication of tensors in the right-hand side of equation (21), we obtain the following relations:

$$\begin{aligned} \frac{\mathrm{d}W_{xx}}{\mathrm{d}t} &= \frac{\mathrm{d}W_{x'x'}}{\mathrm{d}t}\cos(2\varphi) + O_{xx}, \\ \frac{\mathrm{d}W_{xy}}{\mathrm{d}t} &= \frac{\mathrm{d}W_{x'x'}}{\mathrm{d}t}\sin(2\varphi) + O_{xy}, \\ \frac{\mathrm{d}W_{yy}}{\mathrm{d}t} &= -\frac{\mathrm{d}W_{x'x'}}{\mathrm{d}t}\cos(2\varphi) + O_{yy}, \end{aligned} \tag{22}$$

where the terms O_{ik} take into account the volume element rotation relative to the coordinate system. Equations (4), (22), (20), (19) and (14) constitute the model of the polymer plasticity considered in the two-dimensional case.

4. Numerical solution

Equations of the model are solved numerically using finite differences. We write equation of motion (2), for the x component:

$$\frac{\mathrm{d}\upsilon_x}{\mathrm{d}t} = \frac{1}{\rho}\frac{\partial S_{xy}}{\partial y} + \frac{1}{\rho}\left(\frac{\partial S_{xx}}{\partial x} - \frac{\partial P}{\partial x}\right) + \frac{\eta_1}{\rho}\left(\frac{\partial \upsilon_{xx}}{\partial x} + \frac{\partial \upsilon_{xy}}{\partial y}\right). \tag{23}$$

Same for the y component:

$$\frac{\mathrm{d}\upsilon_y}{\mathrm{d}t} = \frac{1}{\rho}\left(\frac{\partial S_{yy}}{\partial y} - \frac{\partial P}{\partial y}\right) + \frac{1}{\rho}\frac{\partial S_{xy}}{\partial x} + \frac{\eta_1}{\rho}\left(\frac{\partial \upsilon_{yx}}{\partial x} + \frac{\partial \upsilon_{yy}}{\partial y}\right). \tag{24}$$

We use the following integral definitions of partial derivatives [16]:

$$\begin{aligned} \frac{\partial F}{\partial x} &= \lim_{A\to 0}\frac{1}{A}\int\limits_C F(\mathbf{n}\times\mathbf{i})\mathrm{d}S \\ \frac{\partial F}{\partial y} &= \lim_{A\to 0}\frac{1}{A}\int\limits_C F(\mathbf{n}\times\mathbf{j})\mathrm{d}S, \end{aligned} \tag{25}$$

where C is boundary of the region A, S is the length of the arc, $\mathbf{n}$ is the normal vector, τ is the tangent vector (figure 2):

$$\mathbf{n} = \frac{\partial x}{\partial n}\mathbf{i} + \frac{\partial y}{\partial n}\mathbf{j} = \frac{\partial y}{\partial S}\mathbf{i} - \frac{\partial x}{\partial S}\mathbf{j}. \tag{26}$$

Using such an expansion of the vector $\mathbf{n}$ (26), integral equation (25) can be represented as follows:

$$\begin{aligned} \int F(\mathbf{n}\times\mathbf{i})\mathrm{d}S &= \int F\frac{\partial y}{\partial S}\mathrm{d}S, \\ \int F(\mathbf{n}\times\mathbf{j})\mathrm{d}S &= -\int F\frac{\partial x}{\partial S}\mathrm{d}S. \end{aligned} \tag{27}$$

Applying this formula to the quadrangle 1, 3, 5, 7, which area is equal to A (figure 3), we obtain for the function F defined in points 1, 3, 5, 7 the following derivatives:

$$\begin{aligned} \frac{\partial F}{\partial x} &= \frac{1}{A}\oint F\mathrm{d}y = \frac{1}{A}\left[F_1(y_3-y_1) + F_2(y_5-y_3) + F_3(y_7-y_5) + F_4(y_1-y_7)\right], \\ \frac{\partial F}{\partial y} &= -\frac{1}{A}\oint F\mathrm{d}x = -\frac{1}{A}\left[F_1(x_3-x_1) + F_2(x_5-x_3) + F_3(x_7-x_5) + F_4(x_1-x_7)\right]. \end{aligned} \tag{28}$$

The equalities (28) are approximate, since the basic formulas (25) are precise at the limit $A \to 0$, but here they are used for the finite rectangle.

Here and below, we assume the following notation: the superscript in parentheses indicates the number of cell, the subscript indicates the node number, and the superscript in square brackets indicates the time step.

Applying formulas (28) for calculating the first spatial derivatives of the deviator components in the center of the cell, we get

$$\begin{aligned} \left(\frac{1}{\rho}\frac{\partial S_{xy}}{\partial y}\right)_0 &= -\frac{1}{m}\left(S_{xy}^{(1)}(x_3-x_1) + S_{xy}^{(2)}(x_5-x_3) + S_{xy}^{(3)}(x_7-x_5) + S_{xy}^{(4)}(x_1-x_7)\right), \\ \left(\frac{1}{\rho}\frac{\partial S_{xx}}{\partial x}\right)_0 &= \frac{1}{m}\left(S_{xx}^{(1)}(y_3-y_1) + S_{xx}^{(2)}(y_5-y_3) + S_{xx}^{(3)}(y_7-y_5) + S_{xx}^{(4)}(y_1-y_7)\right), \\ \left(\frac{1}{\rho}\frac{\partial S_{yy}}{\partial y}\right)_0 &= -\frac{1}{m}\left(S_{yy}^{(1)}(x_3-x_1) + S_{yy}^{(2)}(x_5-x_3) + S_{yy}^{(3)}(x_7-x_5) + S_{yy}^{(4)}(x_1-x_7)\right), \\ \left(\frac{1}{\rho}\frac{\partial S_{xy}}{\partial x}\right)_0 &= \frac{1}{m}\left(S_{xy}^{(1)}(y_3-y_1) + S_{xy}^{(2)}(y_5-y_3) + S_{xy}^{(3)}(y_7-y_5) + S_{xy}^{(4)}(y_1-y_7)\right), \end{aligned} \tag{29}$$

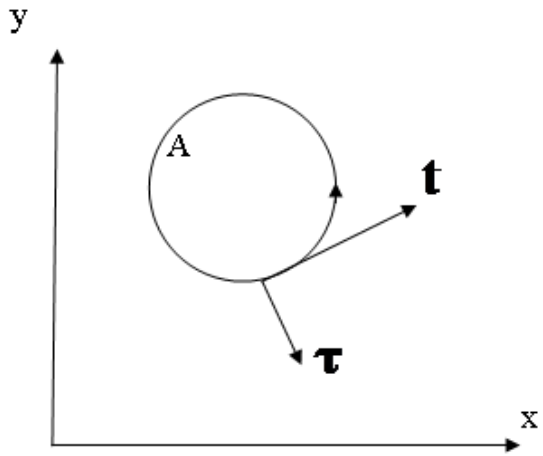

Figure 2. Contour for integration.

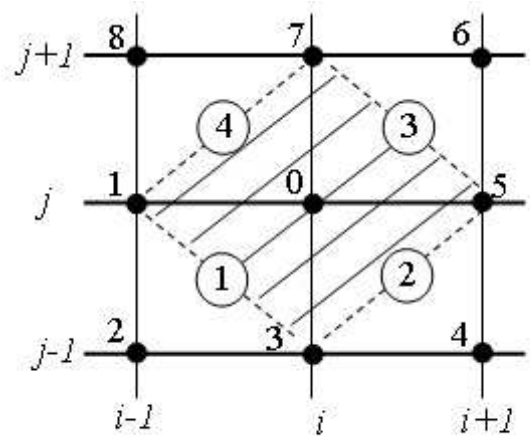

Figure 3. The scheme for the calculation of the derivative components.

where

$$m = \frac{1}{2}\left(m^{(1)} + m^{(2)} + m^{(3)} + m^{(4)}\right). \tag{30}$$

We consider the mass and volume per unit length in the direction of the axis z, then the volume coincides with the area, and will be denoted by the letter V.

Also, using formulas (28), we obtain the first derivative of the components of the pressure in the center of the cell:

$$\begin{aligned}\left(\frac{1}{\rho}\frac{\partial P}{\partial y}\right)_0 &= -\frac{1}{m}\left(P^{(1)}(x_3 - x_1) + P^{(2)}(x_5 - x_3) + P^{(3)}(x_7 - x_5) + P^{(4)}(x_1 - x_7)\right),\\ \left(\frac{1}{\rho}\frac{\partial P}{\partial x}\right)_0 &= \frac{1}{m}\left(P^{(1)}(y_3 - y_1) + P^{(2)}(y_5 - y_3) + P^{(3)}(y_7 - y_5) + P^{(4)}(y_1 - y_7)\right).\end{aligned} \tag{31}$$

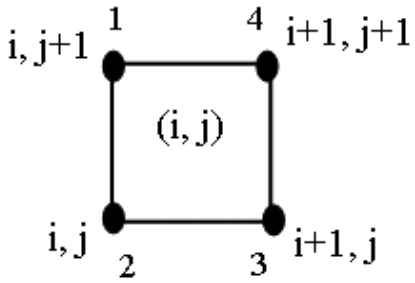

Figure 4. The scheme for calculating the components of the velocity gradient tensor.

Similarly, the spatial derivatives of the velocity gradient in the center of the cell:

$$\begin{aligned}
\left(\frac{1}{\rho}\frac{\partial v_{xy}}{\partial y}\right)_0 &= -\frac{1}{m}\left(v_{xy}^{(1)}(x_3-x_1)+v_{xy}^{(2)}(x_5-x_3)+v_{xy}^{(3)}(x_7-x_5)+v_{xy}^{(4)}(x_1-x_7)\right),\\
\left(\frac{1}{\rho}\frac{\partial v_{xx}}{\partial x}\right)_0 &= -\frac{1}{m}\left(v_{xx}^{(1)}(y_3-y_1)+v_{xx}^{(2)}(y_5-y_3)+v_{xx}^{(3)}(y_7-y_5)+v_{xx}^{(4)}(y_1-y_7)\right),\\
\left(\frac{1}{\rho}\frac{\partial v_{yy}}{\partial y}\right)_0 &= -\frac{1}{m}\left(v_{yy}^{(1)}(x_3-x_1)+v_{yy}^{(2)}(x_5-x_3)+v_{yy}^{(3)}(x_7-x_5)+v_{yy}^{(4)}(x_1-x_7)\right),\\
\left(\frac{1}{\rho}\frac{\partial v_{yx}}{\partial x}\right)_0 &= -\frac{1}{m}\left(v_{yx}^{(1)}(y_3-y_1)+v_{yx}^{(2)}(y_5-y_3)+v_{yx}^{(3)}(y_7-y_5)+v_{yx}^{(4)}(y_1-y_7)\right).
\end{aligned} \tag{32}$$

The components of the velocity gradient tensor in expression (32) are calculated for each grid cell by the following formulas (figure 4):

$$\begin{aligned}
v_{yx} &= \frac{1}{2V}\left((v_1^y-v_3^y)(y_2-y_4)+(v_2^y-v_4^y)(y_3-y_1)\right),\\
v_{yy} &= -\frac{1}{2V}\left((v_1^y-v_3^y)(x_2-x_4)+(v_2^y-v_4^y)(x_3-x_1)\right),\\
v_{xx} &= \frac{1}{2V}\left((v_1^x-v_3^x)(y_2-y_4)+(v_2^x-v_4^x)(y_3-y_1)\right),\\
v_{xy} &= -\frac{1}{2V}\left((v_1^x-v_3^x)(x_2-x_4)+(v_2^x-v_4^x)(x_3-x_1)\right).
\end{aligned} \tag{33}$$

Equations are integrated over time using the explicit Euler method. Particularly, for velocity we have

$$\begin{aligned}
v_x &= v_x^{[n]}+\Delta t\dot{v}_x^{[n]},\\
v_y &= v_y^{[n]}+\Delta t\dot{v}_x^{[n]},
\end{aligned} \tag{34}$$

where t is the step of integration over time.

Similarly one can obtain the following expressions for coordinates

$$\begin{aligned}
x &= x^{[n]}+\Delta t v_x^{[n]},\\
y &= y^{[n]}+\Delta t v_y^{[n]}.
\end{aligned} \tag{35}$$

Formulas (34) and (35) are applied to all grid nodes $i = 1, \ldots, k$, $j = 1, \ldots, m$.

For the internal energy equation, we can rewrite the equation (3):

$$\rho\frac{\mathrm{d}E}{\mathrm{d}t} = -P\upsilon_{kk} + S_{ik}\upsilon_{ik}. \tag{36}$$

Multiplying by $V\mathrm{d}t$, we get

$$m\Delta E = -P^{[n]}\Delta V + W, \tag{37}$$

where W is the power connected with the action of the tangential stresses

$$W = S_{ik}\upsilon_{ik}\Delta tV. \tag{38}$$

As a result, we have

$$E(t) = E^{[n]} + \left(-P^{[n]}\left(V - V^{[n]}\right) + W\right)m^{-1}, \tag{39}$$

where

$$W = \left(S_{xx}\upsilon_{xx} + S_{yy}\upsilon_{yy} + \frac{1}{2}S_{xy}\left(\upsilon_{xy} + \upsilon_{yx}\right)\right)\Delta tV. \tag{40}$$

For the strain tensor

$$u_{ik}(t) = u_{ik}^{[n]} + \Delta t\frac{1}{2}\left(\upsilon_{ik} + \upsilon_{ki}\right), \tag{41}$$

writing its components, we obtain the following

$$\begin{aligned} u_{xx}(t) &= u_{xx}^{[n]} + \Delta t\upsilon_{xx}, \\ u_{yy}(t) &= u_{yy}^{[n]} + \Delta t\upsilon_{yy}, \\ u_{xy}(t) &= u_{xy}^{[n]} + \Delta t\frac{1}{2}\left(\upsilon_{xy} + \upsilon_{yx}\right). \end{aligned} \tag{42}$$

The time step is chosen according to the Courant condition:

$$\Delta\tau = K\min\left(\frac{V}{c_S}\right), \tag{43}$$

where the minimum is taken over all cells, the constant $K \approx 0.01$.

These equations should be supplemented by equation of state of the materials in question and equations (34), (35), (39), (41), thus one can obtain a complete system that allows describing the deformation of PMMA.

5. Comparison of the simulation results with the experimental data

Standard test of the material properties is the flat high-velocity impact of the flyer plate on the target plate [17]. Unloading wave is formed in the impactor after the circulation of the shock wave, which is then propagating into the sample behind the shock wave. In the experiments [3], the shock wave propagates through the sample of the initial thickness of 6.35 mm; the rear surface of the sample is attached to the window. The initial thickness of the impactor is also 6.35 mm. Material of both the impactor and the target is PMMA. A continuous registration of velocity of the rear surface of samples $u_{\mathrm{fs}}(t)$ for various impactor velocities was realized in the experiments [3]. Arrival of the shock wave front leads to the increase of the rear surface velocity. Arrival of the unloading wave on the sample rear surface causes a decrease in speed.

Results of numerical modeling with use of the Maxwell model in comparison with the experimental data [3] are presented in figure 5. Impactor of the initial thickness of 6.35 mm extends along the x-axis. The initial thickness of the sample (target) is taken three times longer

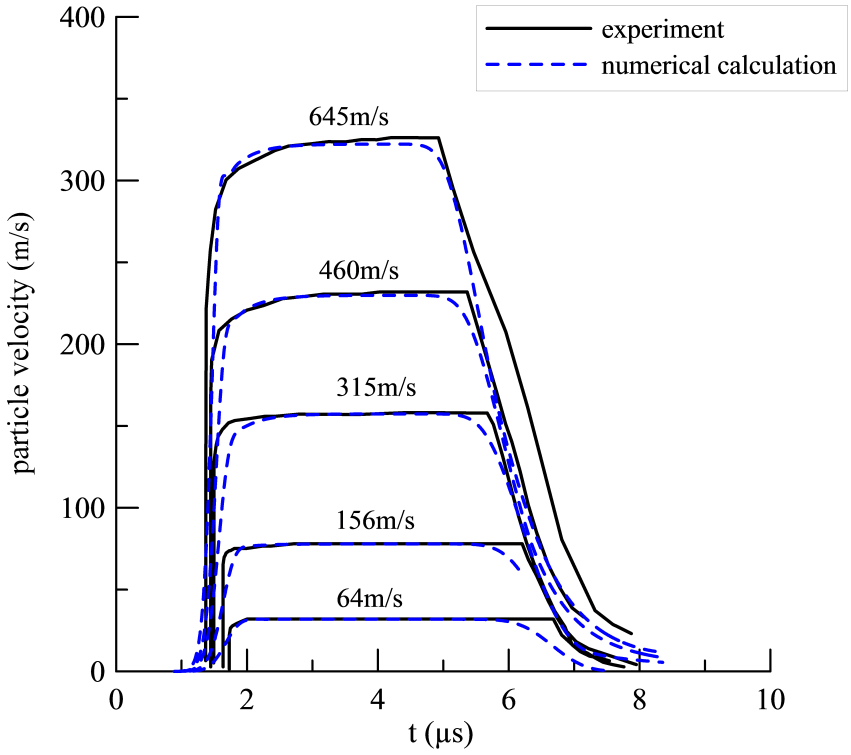

Figure 5. Velocity profiles on the rear surface of PMMA samples: solid lines correspond to the data from experiments [3]; dashed lines are from our calculations with use of Maxwell model.

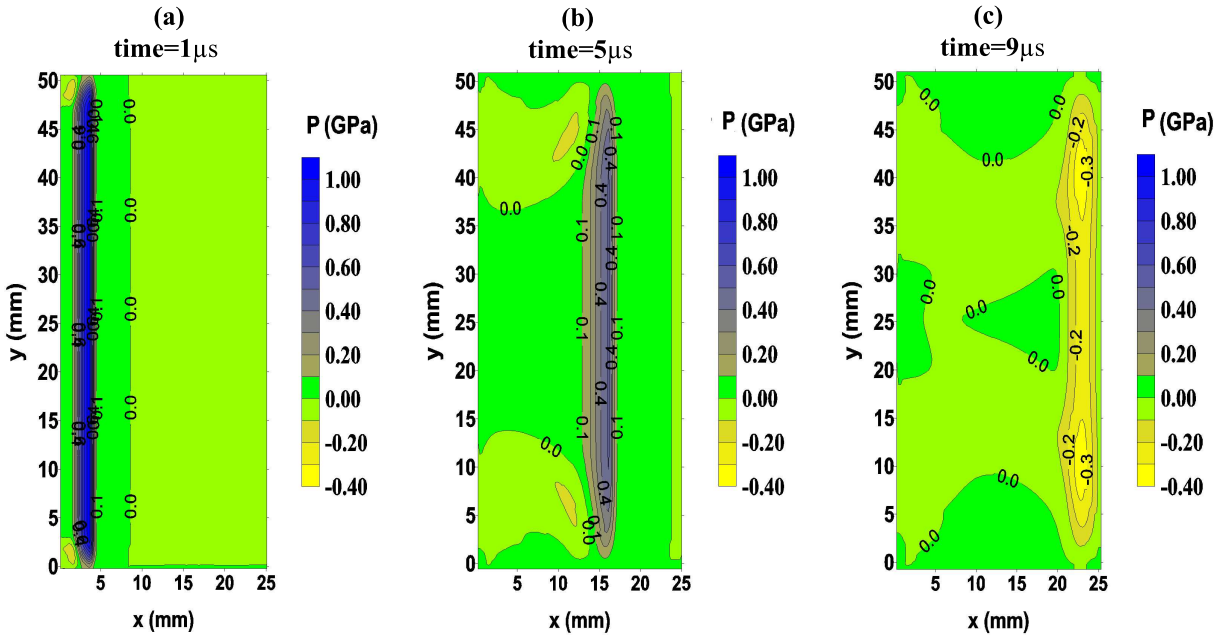

Figure 6. Spatial distribution of pressure.

to avoid the influence of the release wave from the free surface. The height of the sample is taken twice to prevent unloading wave affects in the central part of the target. The size of the

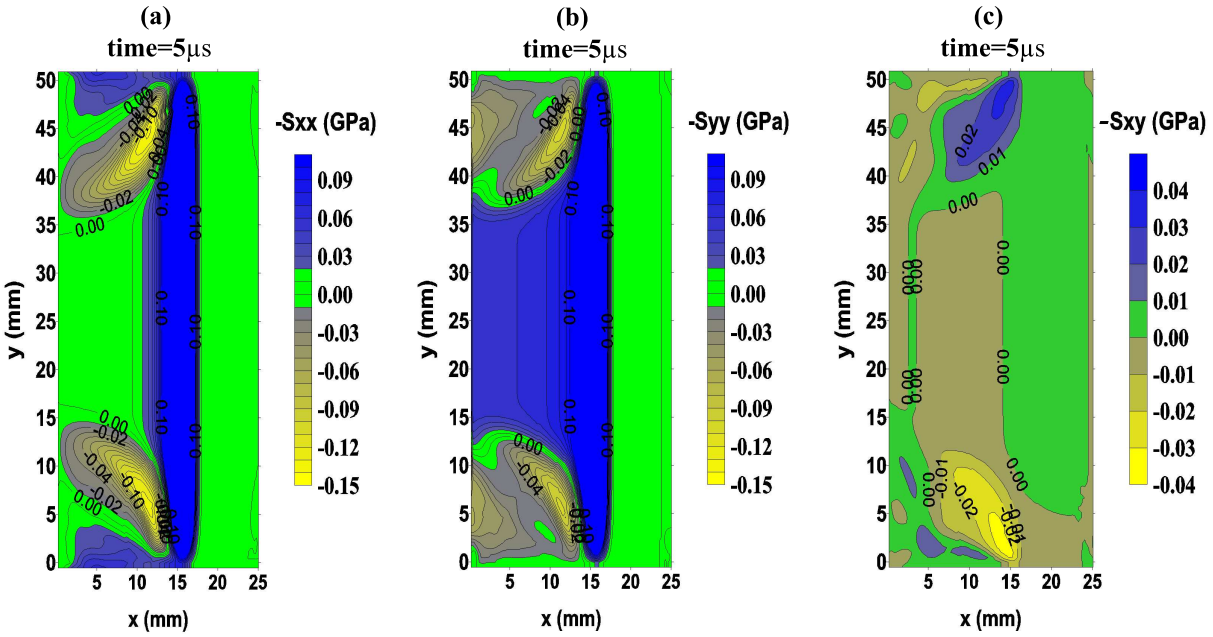

Figure 7. Spatial distribution of component of deviator stress.

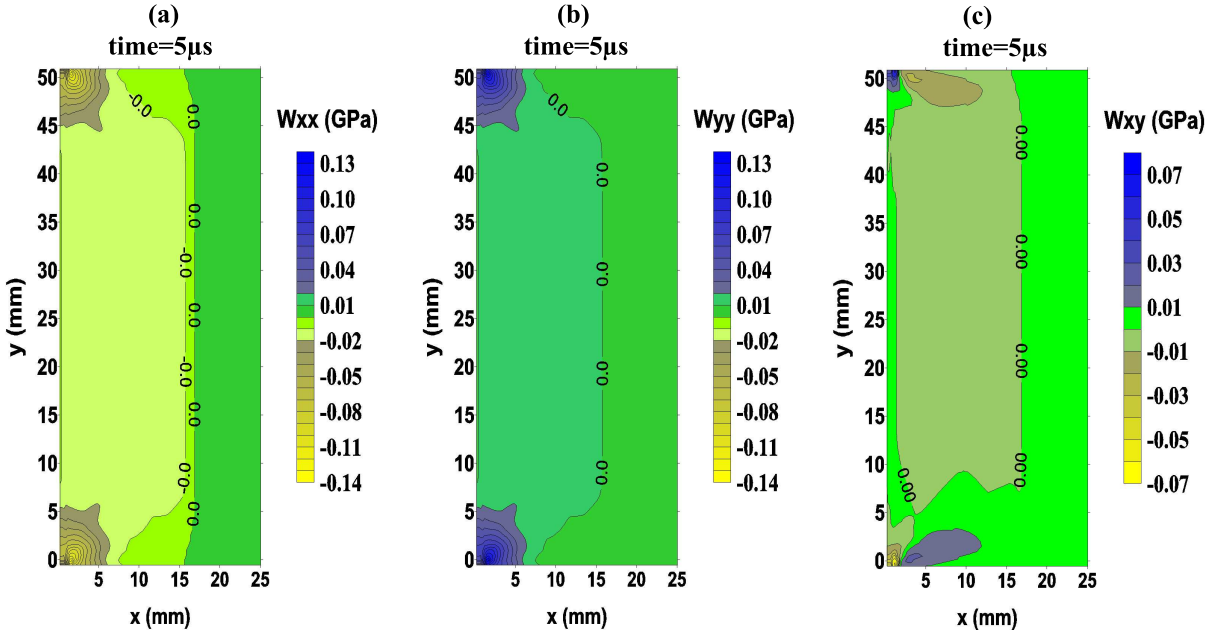

Figure 8. Spatial distribution of components tensor of plastic deformation.

computational domain is 25 mm × 50 mm. Numerical grid of 100 × 200 cells is used in the calculations.

Wave profile is characterized by the initially sharp growth (during the time of the order of nanoseconds) of substance velocity to the value of about two-thirds of the maximal value. This is followed by a smooth increase of the substance velocity to a peak value, and then the velocity remains constant for some time until the arrival of the unloading wave. A good agreement of the calculated and experimental data for the shock wave front is observed in figure 5; as for the

unloading wave, the correspondence is considerably worse. The results presented in figure 5 are calculated with the following parameters of Maxwell model: $G = 1.5$ GPa [18], $\tau = 0.4$ μs, $y_b = 38$ MPa. These parameters correspond to the best coincidence with the experimental data. The results of our calculations qualitatively correspond to the results of modeling [19, 20], which are also obtained with the use of Maxwell model.

Figure 6–8 shows the spatial distribution of physical quantities. The problem is in the plane impingement of the impactor and the target plates with velocity of 645 m/s. The material of the both impactor and target is PMMA; the initial thickness of the impactor is 6.35 mm; the initial thickness of the target is 18.65 mm, the initial height of the both is 50 mm.

Figure 6 shows the spatial distribution of pressure for three time instants: 1 μs, 5 μs and 9 μs. The graph shows the propagation of a shock wave into the target along the x axis upon time. Figures 6a and 6b show how the shock wave emerges and run; figure 6c corresponds to the moment of the negative pressure appearance. Figure 7 shows the spatial distribution of the components of the stress deviator for 5 μs time instant. Figure 8 shows the spatial distribution of plastic strain tensor components at 5 μs.

6. Conclusions

Using Maxwell model of the viscoelastic medium, we perform 2D simulation of impingement of two PMMA plates. Parameters of the Maxwell model are chosen by comparison with the experimental data on the high-velocity impact in order to fit the modeling results with the measured profiles of the free-surface velocity.

Maxwell model with the constant relaxation time allows us to describe the structure of the shock wave front, the unloading wave is described significantly worse. Comparison of calculated results with available experimental data is presented. Graphs of the spatial distribution of physical quantities such as the pressure, component of deviator stress, components tensor of plastic deformation are shown. The results presented indicate the correctness of the code realization of the model.

Acknowledgments

The work is supported by the Ministry of Education and Science of the Russian Federation (state task 3.1334.2014/K), by grants from the President of the Russian Federation (MD-7481.2016.1, NSh-10174.2016.2) and the Russian Foundation for Basic Research (project 14-08-00967).

References

[1] Wilkins M L 1963 *Calculation of Elastic-Plastic Flow* (California: Univ. California Lawrence Radiation Lab.)
[2] Liddiard Jr T P 1965 *Fourth Symposium on Detonation* p 214
[3] Barker L M and Hollenbach R E 1970 *J. Appl. Phys.* **41** 4208–4226
[4] Arzhakov M S, Lukovkin G M and Arzhakov S A 2002 *Chem. Phys. Rep.* **382** 1–4
[5] Geras'kin A A, Khishchenko K V, Krasyuk I K, Pashinin P P, Semenov A Yu and Vovchenko V I 2009 *Contrib. Plasma Phys.* **49** 451–454
[6] Abrosimov S A, Bazhulin A P, Voronov V V, Geras'kin A A, Krasyuk I K, Pashinin P P, Semenov A Yu, Stuchebryukhov I A, Khishchenko K V and Fortov V E 2013 *Quantum Electron.* **43** 246–251
[7] Krasyuk I K, Pashinin P P, Semenov A Yu, Khishchenko K V and Fortov V E 2016 *Laser Phys.* **26** 094001
[8] Zeldovich Ya B and Raizer Yu P 2002 *Physics of Shock Waves and High-Temperature Hydrodynamic Phenomena* (New York: Dover Publication Inc. Mineola)
[9] McQueen R G and March D 1962 *J. Appl. Phys.* **33** 654–665
[10] Kulikovskiy A G, Pogorelov N V and Semenov A Yu 2012 *Mathematical Problems of Numerical Solving Hyperbolic Systems of Equations* (Moscow: FIZMATLIT)
[11] Popova T V, Mayer A E and Khishchenko K V 2015 *J. Phys.: Conf. Ser.* **653** 012045
[12] Landau L D and Lifshitz E M 1987 *Fluid Mechanics* (Oxford: Elsevier)
[13] Lomonosov I V, Fortov V E and Khishchenko K V 1995 *Khim. Fiz.* **14** 47–52
[14] Khishchenko K V, Lomonosov I V and Fortov V E 1996 *Shock Compression of Condensed Matter—1995* ed Schmidt S C and Tao W C (New York: AIP) pp 125–128

[15] Landau L D and Lifshitz E M 1986 *Theory of Elasticity* (Oxford: Elsevier)
[16] Reddick H W and Miller F H 1955 *Advanced Mathematics for Engineers* (New York: Wiley)
[17] Kanel G I, Fortov V E and Razorenov S V 2007 *Phys. Usp.* **50** 771–791
[18] Farshad M, Wildenberg M W and Fliieler P 1997 *Mater. Struct.* **30** 377–382
[19] Merzhievsky L A and Voronin M S 2012 *Proc. Altai State Univ.* **1** 95–98
[20] Merzhievsky L A and Voronin M S 2012 *Combust., Explos. Shock Waves* **48** 226–235